Physica B 412 (2013) 112–118

Contents lists available at SciVerse ScienceDirect

Physica B

journal homepage: www.elsevier.com/locate/physb

# Low temperature acoustic polaron localization

Riccardo Fantoni *

*Dipartimento di Scienze dei Materiali e Nanosistemi, Università Ca' Foscari Venezia, Calle Larga S. Marta DD2137, I-30123 Venezia, Italy*

ARTICLE INFO

*Article history:*
Received 10 October 2012
Received in revised form
12 December 2012
Accepted 21 December 2012
Available online 27 December 2012

*Keywords:*
Acoustic polaron
Path integral Monte Carlo simulation
Localization

ABSTRACT

We calculate the properties of an acoustic polaron in three dimensions in thermal equilibrium at a given low temperature using the path integral Monte Carlo method. The specialized numerical method used is described in full details, thus complementing our previous paper [R. Fantoni, Phys. Rev. B 86 (2012) 144304], and it appears to be the first time it has been used in this context. Our results are in favor of the presence of a phase transition from a localized state to an extended state for the electron as the phonon–electron coupling constant decreases. The phase transition manifests itself with a jump discontinuity in the potential energy as a function of the coupling constant and it affects the properties of the path of the electron in imaginary time: In the weak coupling regime the electron is in an extended state whereas in the strong coupling regime it is found in a self-trapped state.



## 1. Introduction

An electron in a ionic crystal polarizes the lattice in its neighborhood. An electron moving with its accompanying distortion of the lattice has sometimes been called a "polaron" [1,2]. Since 1933 Landau addresses the possibility whether an electron can be self-trapped (ST) in a deformable lattice [3–5]. This fundamental problem in solid state physics has been intensively studied for an optical polaron in an ionic crystal [6–11]. Bogoliubov approached the polaron strong coupling limit with one of his canonical transformations. Feynman used his path integral formalism and a variational principle to develop an all coupling approximation for the polaron ground state [12]. Its extension to finite temperatures appeared first by Osaka [13,14], and more recently by Castrigiano et al. [15–17]. Recently the polaron problem has gained new interest as it could play a role in explaining the properties of the high $T_c$ superconductors [18]. The polaron problem has also been studied to describe an impurity in a Bose–Einstein ultracold quantum gas condensate of atoms [19]. In this context evidence for a transition between free and self-trapped optical polarons is found. For the solid state optical polaron no ST state has been found yet [8,9,11].

The acoustic modes of lattice vibration are known to be responsible for the appearance of the ST state [20,21,1]. Contrary to the optical mode which interacts with the electron through Coulombic force and is dispersionless, the acoustic phonons have a linear dispersion coupled to the electron through a short range potential which is believed to play a crucial role in forming the ST state [22]. Acoustic modes have also been widely studied [1]. Sumi and Toyozawa generalized the optical polaron model by including a coupling to the acoustic modes [23]. Using Feynman's variational approach, they found that the electron is ST with a very large effective mass as the acoustic coupling exceeds a critical value. Emin and Holstein also reached a similar conclusion within a scaling theory [24] in which the Gaussian trial wave function is essentially identical to the harmonic trial action used in the Feynman's variational approach in the adiabatic limit [25].

The ST state distinguishes itself from an extended state (ES) where the polaron has lower mass and a bigger radius. A polaronic phase transition separates the two states with a breaking of translational symmetry in the ST one [1]. The variational approach is unable to clearly assess the existence of the phase transition [1]. In particular Gerlach and Löwen [1] concluded that no phase transition exists in a large class of polarons. The three-dimensional acoustic polaron is not included in the class but Fisher et al. [25] argued that its ground state is delocalized.

In a recent work [26] we employed for the first time a specialized path integral Monte Carlo (PIMC) method [27,28] to the continuous, highly non-local, acoustic polaron problem at low temperature which is valid at all values of the coupling strength and solves the problem exactly (in a Monte Carlo sense). The method differs from previously employed methods [29–35] and hinges on the Lévy construction and the multilevel Metropolis method with correlated sampling. In such work the potential energy was calculated and it was shown that like the effective mass it usefully signals the transition between the ES and the ST state. Properties of ES and ST states were explicitly shown through the numerical simulation.

Aim of the present paper is to give a detailed description of the PIMC method used in that calculation and some additional numerical results in order to complement the brief paper of Ref. [26].

* Tel.: +39 3384570334.
*E-mail addresses:* rfantoni3@gmail.com, rfantoni@ts.infn.it

0921-4526/$ - see front matter © 2012 Elsevier B.V. All rights reserved.
http://dx.doi.org/10.1016/j.physb.2012.12.032

The work is organized as follows: in Section 2 we describe the acoustic polaron model and Hamiltonian, in Section 3 we describe the observables we are going to compute in the simulation, in Section 4 we describe the PIMC numerical scheme employed, in Section 5 we describe the multilevel Metropolis method for sampling the path, in Section 6 we describe the choice of the transition probability and the level action, in Section 7 we describe the correlated sampling. Section 8 is for the results and Section 9 is for final remarks.

## 2. The model

The acoustic polaron can be described by the following quasi-continuous model [7,23]:

$$\hat{H}=\frac{\hat{\boldsymbol{p}}^2}{2m}+\sum_{\boldsymbol{k}}\hbar\omega_k\hat{a}^\dagger_{\boldsymbol{k}}\hat{a}_{\boldsymbol{k}}+\sum_{\boldsymbol{k}}\left(i\Gamma_k\hat{a}_{\boldsymbol{k}}e^{i\boldsymbol{k}\hat{\boldsymbol{x}}}+\text{H.c.}\right). \tag{1}$$

Here $\hat{\boldsymbol{x}}$ and $\hat{\boldsymbol{p}}$ are the electron coordinate and momentum operators respectively and $\hat{a}_{\boldsymbol{k}}$ is the annihilation operator of the acoustic phonon with wave vector $\boldsymbol{k}$. The first term in the Hamiltonian is the kinetic energy of the electron, the second term the energy of the phonons and the third term the coupling energy between the electron and the phonons. The electron coordinate $\boldsymbol{x}$ is a continuous variable, while the phonons wave vector $\boldsymbol{k}$ is restricted by the Debye cut-off $k_o$. The acoustic phonons have a dispersion relation $\omega_k=uk$ ($u$ being the sound velocity) and they interact with the electron of mass $m$ through the interaction vertex $\Gamma_k=\hbar uk_o(S/N)^{1/2}(k/k_o)^{1/2}$ according to the deformation potential analysis of Ref. [36]. $S$ is the coupling constant between the electron and the phonons and $N$ is the number of unit cells in the crystal with $N/V=(4\pi/3)(k_o/2\pi)^3$ by Debye approximation and $V$ is the crystal volume.

Using the path integral representation (see Ref. [12] Section 8.3), the phonon part in the Hamiltonian can be exactly integrated owing to its quadratic form in phonon coordinates, and one can write the partition function for a polaron in thermal equilibrium at an absolute temperature $T$ ($\beta=1/k_BT$, with $k_B$ Boltzmann constant) as follows:

$$Z=\int d\boldsymbol{x}\int_-^{\boldsymbol{x}=\boldsymbol{x}(\hbar\beta)}_{\boldsymbol{x}=\boldsymbol{x}(0)}e^{-(1/\hbar)\mathcal{S}[\boldsymbol{x}(t),\dot{\boldsymbol{x}}(t),t]}\mathcal{D}\boldsymbol{x}(t), \tag{2}$$

where the action $\mathcal{S}$ is given by Ref. [37] [1]

$$\mathcal{S}=\frac{m}{2}\int_0^{\hbar\beta}\dot{\boldsymbol{x}}^2(t)\,dt-\frac{1}{2\hbar}\int_0^{\hbar\beta}dt\int_0^{\hbar\beta}ds\int\frac{d\boldsymbol{k}}{(2\pi)^3}\Gamma_k^2e^{i\boldsymbol{k}\cdot(\boldsymbol{x}(t)-\boldsymbol{x}(s))-\omega_k|t-s|}$$
$$=\mathcal{S}_f+\mathcal{U}. \tag{3}$$

Here $\mathcal{S}_f$ is the *free particle action* and $\mathcal{U}$ is the *inter action* and we denoted with a dot a time derivative as usual. Using dimensionless units $\hbar=m=uk_o=k_B=V=1$ the action becomes

$$\mathcal{S}=\int_0^\beta\frac{\dot{\boldsymbol{x}}^2(t)}{2}\,dt+\int_0^\beta dt\int_0^\beta ds\,V_{\mathit{eff}}(|\boldsymbol{x}(t)-\boldsymbol{x}(s)|,|t-s|), \tag{4}$$

with the electron moving subject to an effective retarded potential

$$V_{\mathit{eff}}=-\frac{S}{2I_D}\int_{q\le1}d\boldsymbol{q}\,qe^{i\sqrt{2/\gamma}\boldsymbol{q}\cdot(\boldsymbol{x}(t)-\boldsymbol{x}(s))-q|t-s|} \tag{5}$$

$$V_{\mathit{eff}}=-\frac{3S}{2}\sqrt{\frac{\gamma}{2}}\frac{1}{|\boldsymbol{x}(t)-\boldsymbol{x}(s)|}\int_0^1dq\,q^2\sin\left(\sqrt{\frac{2}{\gamma}}q|\boldsymbol{x}(t)-\boldsymbol{x}(s)|\right)e^{-q|t-s|}, \tag{6}$$

[1] This is an approximation as $e^{-\beta\omega_k}$ is neglected. The complete form is obtained by replacing $e^{-\omega_k|t-s|}$ by $e^{-\omega_k|t-s|}/(1-e^{-\beta\omega_k})+e^{\omega_k|t-s|}e^{-\beta\omega_k}/(1-e^{-\beta\omega_k})$. But remember that β is large.

where $\boldsymbol{q}=\boldsymbol{k}/k_o$, $I_D=\int_{q\le1}d\boldsymbol{q}=4\pi/3$, and we have introduced a non-adiabatic parameter $\gamma$ defined as the ratio of the average phonon energy, $\hbar uk_o$ to the electron band-width, $(\hbar k_o)^2/2m$. This parameter is of order of $10^{-2}$ in typical ionic crystals with broad band so that the ST state is well-defined [23]. In our simulation we took $\gamma=0.02$. Note that the integral in Eq. (6) can be solved analytically and the resulting function tabulated.

## 3. The observables

In particular the internal energy $E$ of the polaron is given by

$$E=-\frac{1}{Z}\frac{\partial Z}{\partial\beta}=\frac{1}{Z}\int d\boldsymbol{x}\int_-^{}\int e^{-\mathcal{S}}\frac{\partial\mathcal{S}}{\partial\beta}\mathcal{D}\boldsymbol{x}=\left\langle\frac{\partial\mathcal{S}}{\partial\beta}\right\rangle, \tag{7}$$

where the internal energy tends to the ground state energy in the large $\beta\longrightarrow\infty$ limit.

Scaling the Euclidean time $t=\beta t'$ and $s=\beta s'$ in Eq. (4), deriving $\mathcal{S}$ with respect to β, and undoing the scaling, we get

$$\frac{\partial\mathcal{S}}{\partial\beta}=-\frac{1}{\beta}\int_0^\beta\frac{\dot{\boldsymbol{x}}^2}{2}dt-\frac{S}{2I_D}\int_0^\beta dt\int_0^\beta ds$$
$$\times\int_{q\le1}d\boldsymbol{q}\,qe^{i\sqrt{2/\gamma}\boldsymbol{q}\cdot(\boldsymbol{x}(t)-\boldsymbol{x}(s))-q|t-s|}\frac{1}{\beta}(2-q|t-s|), \tag{8}$$

where the first term is the kinetic energy contribution to the internal energy, $\mathcal{K}$, and the last term is the potential energy contribution, $\mathcal{P}$

$$\mathcal{P}=-\frac{3S}{2\beta}\int_0^\beta dt\int_0^\beta ds\int_0^1dq\,q^3\frac{\sin\left(\sqrt{\frac{2}{\gamma}}q|\boldsymbol{x}(t)-\boldsymbol{x}(s)|\right)}{\sqrt{\frac{2}{\gamma}}q|\boldsymbol{x}(t)-\boldsymbol{x}(s)|}e^{-q|t-s|}$$
$$\times(2-q|t-s|). \tag{9}$$

So that

$$E=\langle\mathcal{K}+\mathcal{P}\rangle. \tag{10}$$

An expression for $\mathcal{K}$ not involving the polaron speed, can be obtained by taking the derivative with respect to β after having scaled both the time, as before, and the coordinate $\boldsymbol{x}=\sqrt{\beta}\boldsymbol{x}'$. Undoing the scaling in the end one gets

$$\mathcal{K}=-\frac{S}{4\beta I_D}\int_0^\beta dt\int_0^\beta ds\int_{q\le1}d\boldsymbol{q}\,qe^{i\sqrt{(2/\gamma)}\boldsymbol{q}\cdot(\boldsymbol{x}(t)-\boldsymbol{x}(s))-q|t-s|}$$
$$\times\left[i\sqrt{\frac{2}{\gamma}}\boldsymbol{q}\cdot(\boldsymbol{x}(t)-\boldsymbol{x}(s))\right] \tag{11}$$

$$\mathcal{K}=-\frac{3S}{4\beta}\int_0^\beta dt\int_0^\beta ds\int_0^1dq\,q^3\left[\cos\left(\sqrt{\frac{2}{\gamma}}q|\boldsymbol{x}(t)-\boldsymbol{x}(s)|\right)\right.$$
$$\left.-\frac{\sin\left(\sqrt{\frac{2}{\gamma}}q|\boldsymbol{x}(t)-\boldsymbol{x}(s)|\right)}{\sqrt{\frac{2}{\gamma}}q|\boldsymbol{x}(t)-\boldsymbol{x}(s)|}\right]e^{-q|t-s|}. \tag{12}$$

In the following we will explain how we calculated the potential energy $P=\langle\mathcal{P}\rangle$.

## 4. Discrete path integral expressions

Generally we are interested in calculating the density matrix $\hat{\rho}=\exp(-\beta\hat{H})$ in the electron coordinate basis, namely

$$\rho(\boldsymbol{x}_a,\boldsymbol{x}_b;\beta)=\int_-^{\boldsymbol{x}=\boldsymbol{x}_b}_{\boldsymbol{x}=\boldsymbol{x}_a}e^{-\mathcal{S}}\mathcal{D}\boldsymbol{x}(t). \tag{13}$$

To calculate the path integral, we first choose a subset of all paths. To do this, we divide the independent variable, Euclidean

time, into *steps* of width

$$\tau = \beta/M. \tag{14}$$

This gives us a set of *times*, $t_k = k\tau$ spaced a distance $\tau$ apart between 0 and β with $k = 0,1,2,\ldots,M$.

At each time $t_k$ we select the special point $\boldsymbol{x}_k = \boldsymbol{x}(t_k)$, the $k$-th *time slice*. We construct a path by connecting all points so selected by straight lines. It is possible to define a sum over all paths constructed in this manner by taking a multiple integral over all values of $\boldsymbol{x}_k$ for $k = 1,2,\ldots,M-1$ where $\boldsymbol{x}_0 = \boldsymbol{x}_a$ and $\boldsymbol{x}_M = \boldsymbol{x}_b$ are the two fixed ends. The resulting equation is

$$\rho(\boldsymbol{x}_a,\boldsymbol{x}_b;\beta) = \lim_{\tau\to 0}\frac{1}{A}\int_{-\infty}^{\infty}\int_{-\infty}^{\infty}\cdots\int_{-\infty}^{\infty} e^{-\mathcal{S}}\frac{d\boldsymbol{x}_1}{A}\cdots\frac{d\boldsymbol{x}_{M-1}}{A}, \tag{15}$$

where the normalizing factor $A = (2\pi\tau)^{3/2}$.

The simplest discretized expression for the action can then be written as follows:

$$\mathcal{S} = \sum_{k=1}^{M}\frac{(\boldsymbol{x}_{k-1}-\boldsymbol{x}_k)^2}{2\tau} + \tau^2\sum_{i=1}^{M}\sum_{j=1}^{M} V(t_i,t_j), \tag{16}$$

where $V(t_i,t_j) = V_{eff}(|\boldsymbol{x}_i-\boldsymbol{x}_j|,|i-j|)$ is a symmetric two variables function, $V(s,t) = V(t,s)$. In our simulation we tabulated this function taking $|\boldsymbol{x}_i-\boldsymbol{x}_j| = 0,0.1,0.2,\ldots,10$ and $|i-j| = 0,1,\ldots,M$.

In writing Eq. (16) we used the following approximate expressions:

$$\dot{\boldsymbol{x}}_k = \frac{\boldsymbol{x}_k-\boldsymbol{x}_{k-1}}{\tau} + O(\tau), \tag{17}$$

$$\int_{t_{k-1}}^{t_k}\dot{\boldsymbol{x}}^2(t)\,dt = \dot{\boldsymbol{x}}_k^2\tau + O(\tau^2), \tag{18}$$

$$\int_{t_{i-1}}^{t_i}\int_{t_{j-1}}^{t_j} V(s,t)\,ds\,dt = V(t_i,t_j)\tau^2 + O(\tau^3). \tag{19}$$

If we take $V=0$ in Eq. (16) the $M-1$ Gaussian integrals in Eq. (15) can be done analytically. The result is the exact free particle density matrix

$$\rho_f(\boldsymbol{x}_a,\boldsymbol{x}_b;\beta) = (2\pi\beta)^{-3/2}e^{(1/2\beta)(\boldsymbol{x}_a-\boldsymbol{x}_b)^2}. \tag{20}$$

Thus approximations (17) and (18) allow us to rewrite the polaron density matrix as follows:

$$\rho(\boldsymbol{x}_a,\boldsymbol{x}_b;\beta) = \int\cdots\int d\boldsymbol{x}_1\cdots d\boldsymbol{x}_{M-1}\;\rho_f(\boldsymbol{x}_a,\boldsymbol{x}_1;\tau)\cdots\rho_f(\boldsymbol{x}_{M-1},\boldsymbol{x}_M;\tau) \times e^{\tau^2\sum_i\sum_j V(t_i,t_j)}. \tag{21}$$

In the next section we will see that this expression offers a useful starting point for the construction of an algorithm for the sampling of the path: the Lévy construction and the analogy with classical polymer systems or the classical isomorphism described in Ref. [27].

The partition function is the trace of the density matrix

$$Z = \int d\boldsymbol{x}\,\rho(\boldsymbol{x},\boldsymbol{x};\beta). \tag{22}$$

This restrict the path integral to an integral over closed paths only. In other words the paths we need to consider in calculating $Z$ (and hence $F$) are closed by the *periodic boundary condition*, $\boldsymbol{x}_M = \boldsymbol{x}_0 = \boldsymbol{x}$.

To calculate the internal energy we need then to perform the following $M$-dimensional integral:

$$E = \frac{1}{Z}\int_{-\infty}^{\infty}\int_{-\infty}^{\infty}\cdots\int_{-\infty}^{\infty} d\boldsymbol{x}_0\,d\boldsymbol{x}_1\;\cdots\;d\boldsymbol{x}_{M-1}\,e^{-\mathcal{S}}(\mathcal{P}+\mathcal{K})\Big|_{\boldsymbol{x}_M=\boldsymbol{x}_0}. \tag{23}$$

To do this integral we use the Monte Carlo simulation technique described next.

## 5. Sampling the path

The total configuration space to be integrated over is made of elements $s = [\boldsymbol{x}_0,\boldsymbol{x}_1,\ \ldots,\boldsymbol{x}_M]$ where $\boldsymbol{x}_k$ are the path time slices subject to the periodic boundary condition $\boldsymbol{x}_M = \boldsymbol{x}_0$. In the simulation we wish to sample these elements from the probability distribution

$$\pi(s) = \frac{e^{-\mathcal{S}}}{Z}, \tag{24}$$

where the partition function $Z$ normalizes the function π in this space.

The idea is to find an efficient way to move the path in a random walk sampled by π, through configuration space.

In order to be able to make the random walk diffuse fast through configuration space, as $\tau$ decreases, is necessary to use multislices moves [27].

In our simulation we chose to use the bisection method (a particular multilevel Monte Carlo sampling method [27]). That is how an $l$ levels move is constructed. Clip out of the path $m = 2^l$ subsequent time slices $\boldsymbol{x}_i,\boldsymbol{x}_{i+1},\ldots,\boldsymbol{x}_{i+m}$ (choosing $i$ randomly). In the first level we keep $\boldsymbol{x}_i$ and $\boldsymbol{x}_{i+m}$ fixed and, following Lévy construction for a Brownian bridge [38], we move the bisecting point at $i+m/2$ to:

$$\boldsymbol{x}_{i+m/2} = \frac{\boldsymbol{x}_i+\boldsymbol{x}_{i+m}}{2} + \boldsymbol{\eta}, \tag{25}$$

where $\boldsymbol{\eta}$ is a normally distributed random vector with mean zero and standard deviation $\sqrt{\tau m/4}$. As shown in next section this kind of transition rule samples the path using a transition probability distribution $T \propto \exp(-\mathcal{S}_f)$. Thus we will refer to it as *free particle sampling*.

Having sampled $\boldsymbol{x}_{i+m/2}$, we proceed to the second level bisecting the two new intervals $(0,i+m/2)$ and $(i+m/2,i+m)$ generating points $\boldsymbol{x}_{i+m/4}$ and $\boldsymbol{x}_{i+3m/4}$ with the same algorithm. We continue recursively, doubling the number of sampled points at each level, stopping only when the time difference of the intervals is $\tau$.

In this way we are able to partition the full configuration $s$ into $l$ levels, $s = (s_0,s_1,\ldots,s_l)$ where $s_0 = [\boldsymbol{x}_0,\ldots,\boldsymbol{x}_i,\boldsymbol{x}_{i+m},\ldots,\boldsymbol{x}_{M-1}]$, unchanged; $s_1 = [\boldsymbol{x}_{i+m/2}]$, changed in level 1; $s_2 = [\boldsymbol{x}_{i+m/4},\boldsymbol{x}_{i+3m/4}]$, changed in level 2; …; $s_l = [\boldsymbol{x}_{i+1},\boldsymbol{x}_{i+2},\ldots,\boldsymbol{x}_{i+m-1}]$ changed in level $l$.

To construct the random walk we use the multilevel Metropolis method [39,40,27]. Call $(s'_1,\ldots,s'_l)$ the new trial positions in the sense of a Metropolis rejection method, the unprimed ones are the corresponding old positions with $s_0 = s'_0$.

In order to decide if the sampling of the path should continue beyond level $k$, we need to construct the probability distribution $\pi_k$ for level $k$. This, usually called the *level action*, is a function of $s_0,s_1\ldots,s_k$ proportional to the reduced distribution function of $s_k$ conditional on $s_0,s_1\ldots,s_{k-1}$. The optimal choice for the level action would thus be

$$\pi_k^\star(s_0,s_1\ldots,s_k) = \int ds_{k+1}\ldots\,ds_l\,\pi(s). \tag{26}$$

This is only a guideline. Non-optimal choices will lead to slower movement through configuration space. One needs to require only that feasible paths (closed ones) have non-zero level action, and that the action at the last level be exact

$$\pi_l(s_0,s_1,\ldots,s_l) = \pi(s). \tag{27}$$

Given the level action $\pi_k(s)$ the optimal choice for the transition probability $T_k(s_k)$, for $s_k$ contingent on the levels already sampled, is given by

$$T_k^\star(s_k) = \frac{\pi_k(s)}{\pi_{k-1}(s)}. \tag{28}$$

One can show that $T_k^\star$ will be a normalized probability if and only if $\pi_k$ is chosen as in Eq. (26). In general one need to require only

that $T_k$ be a probability distribution non-zero for feasible paths. In our simulation we used the free particle transition probability of the Lévy construction as a starting point for a more efficient correlated sampling that will be described in a later section.

Once the partitioning and the sampling rule are chosen, the sampling proceeds past level $k$ with probability

$$A_k(s') = \min\left[1, \frac{T_k(s_k)\pi_k(s')\pi_{k-1}(s)}{T_k(s'_k)\pi_k(s)\pi_{k-1}(s')}\right]. \tag{29}$$

That is we compare $A_k$ with a uniformly distributed random number in (0,1), and if $A_k$ is larger, we go on to sample the next level. If $A_k$ is smaller, we make a new partitioning of the initial path, and start again from level 1. Here $\pi_0$ needed in the first level can be set equal to 1, since it will cancel out of the ratio.

This acceptance probability has been constructed so that it satisfies a form of "detailed balance" for each level $k$

$$\frac{\pi_k(s)}{\pi_{k-1}(s)} T_k(s'_k) A_k(s') = \frac{\pi_k(s')}{\pi_{k-1}(s')} T_k(s_k) A_k(s). \tag{30}$$

The moves will always be accepted if the transition probabilities and level actions are set to their optimal values.

The total transition probability for a trial move making it through all $l$ levels is

$$P(s \to s') = \prod_{k=1}^{l} T_k(s') A_k(s'). \tag{31}$$

By multiplying Eq. (30) from $k=1$ to $k=l$ and using Eq. (27), one can verify that the total move satisfy the detailed balance condition

$$\pi(s) P(s \to s') = \pi(s') P(s' \to s). \tag{32}$$

Thus if there are no barriers or conserved quantities that restrict the walk to a subset of the full configuration space (i.e. assuming the random walk to be ergodic) the algorithm will asymptotically converge to $\pi$, independent of the particular form chosen for the transition probabilities, $T_k$, and the level actions, $\pi_k$ [41]. We will call *equilibration time* the number of moves needed in the simulation to reach convergence.

Whenever the last level is reached, one calculates the properties ($\mathcal{K}$ and $\mathcal{P}$) on the new path $s'$, resets the initial path to the new path, and start a new move. We will call Monte Carlo step (MCS) any attempted move.

## 6. Choice of $T_k$ and $\pi_k$

In our simulation we started moving the path with the Lévy construction described in the preceding section. We will now show that this means that we are sampling an approximate $T^\star$ with free particle sampling.

For the free particle case ($\mathcal{U}=0$) one can find analytic expressions for the optimal level action $\pi_k^\star$ and the optimal transition rule $T_k^\star$. For examples for the first level, Eq. (26) gives

$$\pi_1^\star(\boldsymbol{x}_{i+m/2}) \propto \rho_f(\boldsymbol{x}_i, \boldsymbol{x}_{i+m/2}; \tau m/2) \rho_f(\boldsymbol{x}_{i+m/2}, \boldsymbol{x}_{i+m}; \tau m/2), \tag{33}$$

$$\pi_1^\star(\boldsymbol{x}_{i+m/2}) \propto e^{(1/m\tau)(\boldsymbol{x}_i - \boldsymbol{x}_{i+m/2})^2} e^{(1/m\tau)(\boldsymbol{x}_{i+m/2} - \boldsymbol{x}_{i+m})^2}, \tag{34}$$

$$\pi_1^\star(\boldsymbol{x}_{i+m/2}) \propto e^{(2/m\tau)[\boldsymbol{x}_{i+m/2} - ((\boldsymbol{x}_i + \boldsymbol{x}_{i+m})/2)]^2}. \tag{35}$$

This justify the Lévy construction and shows that it exactly samples the free particle action (i.e. $A_k=1$ for all $k$'s). This also imply that for the interacting system we can introduce a *level inter action*, $\tilde{\pi}_k$ such that

$$\tilde{\pi}_k = \int ds_{k+1} \dots ds_l \, \tilde{\pi}(s), \tag{36}$$

with

$$\tilde{\pi}(s) = \frac{e^{-\mathcal{U}}}{Z}. \tag{37}$$

So that the acceptance probability will have the simplified expression

$$A_k(s') = \min\left[1, \frac{\tilde{\pi}_k(s')\tilde{\pi}_{k-1}(s)}{\tilde{\pi}_k(s)\tilde{\pi}_{k-1}(s')}\right]. \tag{38}$$

For the $k$-th level inter action we chose the following expression:

$$\tilde{\pi}_k \propto \exp\left[-(\tau\ell_k)^2 \sum_{i=1}^{[M/\ell_k]} \sum_{j=1}^{[M/\ell_k]} V(i\ell_k\tau, j\ell_k\tau)\right], \tag{39}$$

where $\ell_k = m/2^k$. In the last level $\ell_l = 1$ and the level inter action $\tilde{\pi}_l$ reduces to the exact inter action $\tilde{\pi}$ thus satisfying Eq. (27).

It is important to notice that during the simulation we never need to calculate the complete level inter action since in the acceptance probabilities enter only ratios of level inter actions calculated on the old and on the new path. For example if for the move we clipped out the interval $t_i, \dots, t_{i+m}$ with $i+m < M$,[2] we have

$$\ln \frac{\tilde{\pi}_k(s')}{\tilde{\pi}_k(s)} = -(\tau\ell_k)^2 \left\{ \sum_{m=0}^{2^k} \sum_{n=0}^{2^k} V(t_i + m\ell_k\tau, t_i + n\ell_k\tau) + \sum_{m=1}^{i-1} \sum_{n=0}^{2^k} V(m\ell_k\tau, t_i + n\ell_k\tau) + \sum_{m=i+m+1}^{M} \sum_{n=0}^{2^k} V(m\ell_k\tau, t_i + n\ell_k\tau) \right\}, \tag{40}$$

which is computationally much cheaper than Eq. (39).

## 7. Correlated sampling

When the path reaches equilibrium (i.e. $P(s \to s') \approx \pi(s')$) if we calculate

$$\sigma(t_0/\tau) = \sqrt{\left\langle \left[\boldsymbol{x}(t) - \left(\frac{\boldsymbol{x}(t+t_0) + \boldsymbol{x}(t-t_0)}{2}\right)\right]^2 \right\rangle}, \tag{41}$$

we see that these deviations are generally smaller than the free particle standard deviations used in the Lévy construction (see Fig. 1)

$$\sigma_f(\ell_k) = \sqrt{\ell_k \tau / 2}. \tag{42}$$

As Fig. 1 shows, the discrepancy gets bigger as $\ell_k$ increases.

We thus corrected the sampling rule for the correct deviations. For example for the first level we used

$$T_1(\boldsymbol{x}_{i+m/2}) \propto e^{-((\boldsymbol{x}_{i+m/2} - \overline{\boldsymbol{x}})^2)/2\sigma^2(m/2)}, \tag{43}$$

where $\overline{\boldsymbol{x}} = (\boldsymbol{x}_i + \boldsymbol{x}_{i+m})/2$. Since the level action is given by

$$\pi_1(\boldsymbol{x}_{i+m/2}) \propto e^{-((\boldsymbol{x}_{i+m/2} - \overline{\boldsymbol{x}})^2)/2\sigma_f^2(m/2)} \tilde{\pi}_1(\boldsymbol{x}_{i+m/2}), \tag{44}$$

we can define a function

$$P_1 \propto e^{-(\boldsymbol{x}_{i+m/2} - \overline{\boldsymbol{x}})^2 / 2[1/\sigma^2(m/2) - 1/\sigma_f^2(m/2)]} \tag{45}$$

and write the acceptance probability

$$A_1(s') = \min\left[1, \frac{P_1(s)}{P_1(s')} \frac{\tilde{\pi}_1(s')\tilde{\pi}_0(s)}{\tilde{\pi}_1(s)\tilde{\pi}_0(s')}\right], \tag{46}$$

which is a generalization of Eq. (38).

[2] When $i+m \geq M$ there is a minor problem with the periodic boundary conditions and Eq. (40) will change.

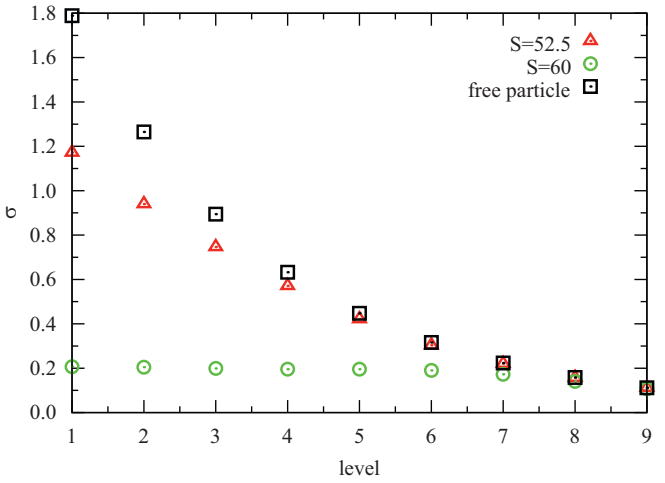


**Fig. 1.** Shows the deviations (41) for a simulation with $S=60$ and $S=52.5$, $\tau=0.025$, $l=9$. The free particle standard deviations (42) are plotted for comparison. For $S=60$ the path is localized while for $S=52.5$ is unlocalized i.e. closer to the free particle path.

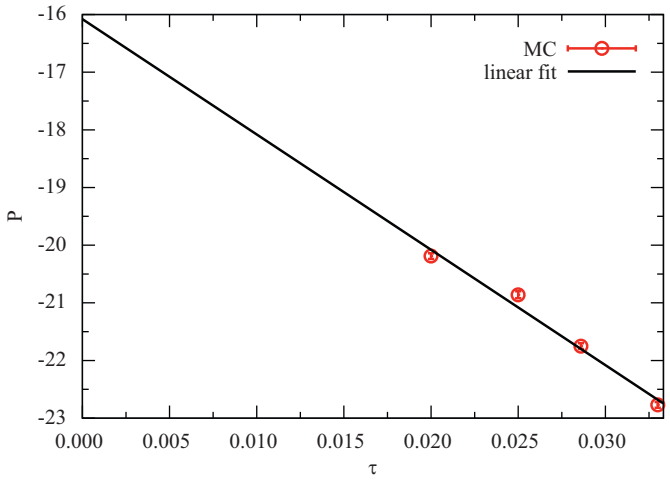


**Fig. 2.** Shows the time step, $\tau$, extrapolation for the potential energy, $P=\langle\mathcal{P}\rangle$. We run at $\beta=15$, $\gamma=0.02$, and $S=60$. The extrapolated value to the continuum limit is in this case $P=-16.1(5)$ which is in good agreement with the result of Ref. [33].

We maintain the acceptance ratios in [0.15, 0.65] by decreasing (or increasing) the number of levels in the multilevel algorithm as the acceptance ratios becomes too low (or too high).

In the Appendix we report some remarks on the error analysis in our MC simulations.

## 8. Numerical results

We simulated the acoustic polaron fixing the adiabatic coupling constant $\gamma=0.02$ and the inverse temperature $\beta=15$. Such temperature is found to be well suited to extract close to ground state properties of the polaron. The path was $M$ time slices long and the time step was $\tau=\beta/M$. For a given coupling constant $S$ we computed the potential energy $P$ extrapolating (with a linear $\chi$ square fit) to the continuum time limit, $\tau\to 0$, three points corresponding to time-steps chosen in the interval $\tau\in[1/100,1/30]$. An example of extrapolation is shown in Fig. 2 for the particular case $\beta=15$, $\gamma=0.02$, and $S=60$.

In Fig. 5 and Table 1 we show that the results for the potential energy as a function of the coupling strength. With the coupling constant $S=52.5$ we generated the equilibrium path which turns out to be unlocalized (see Fig. 4). Changing the coupling constant to $S=60$ and taking the unlocalized path as the initial path we sow the phase transition described in Fig. 3. The path after the phase transition is localized (see Fig. 4).

Note that since $S$ and $\tau$ appear in the combination $S\tau^2$ in $\mathcal{U}$ (and $S\tau$ in F) the same phase transition from an ES to a ST state will be observed increasing the temperature. With the same Hamiltonian we are able to describe two very different behavior of the acoustic polaron as the temperature changes.

In Fig. 5 we show that the behavior of the potential energy as a function of the coupling strength. The numerical results suggest the existence of a phase transition between two different regimes which corresponds to the so-called ES and ST states for the weak and strong coupling region respectively. We found that paths related to ES and ST are characteristically distinguishable. Two typical paths for the ES and ST regimes involved in Fig. 5 are illustrated in Fig. 4. The path in ES state changes smoothly in a large time scale, whereas the path in ST state do so abruptly in a small time scale with a much smaller amplitude which is an indication that the polaron hardly moves. The local fluctuations in the results for the potential energy have an autocorrelation

**Table 1**
MC results for $P$ as a function of $S$ at $\beta=15$ and $\gamma=0.02$ displayed in Fig. 5. The runs where made of $5\times10^5$ MCS (with $5\times10^4$ MCS for the equilibration) for the ES states and $5\times10^6$ MCS (with $5\times10^5$ MCS for the equilibration) for the ST states.

| $S$ | $P$ |
|---|---|
| 10 | −0.573(8) |
| 20 | −1.17(2) |
| 30 | −1.804(3) |
| 40 | −2.53(3) |
| 50 | −3.31(4) |
| 53.5 | −3.61(1) |
| 55 | −11.4(3) |
| 60 | −16.1(5) |
| 70 | −23.3(3) |
| 80 | −30.0(3) |

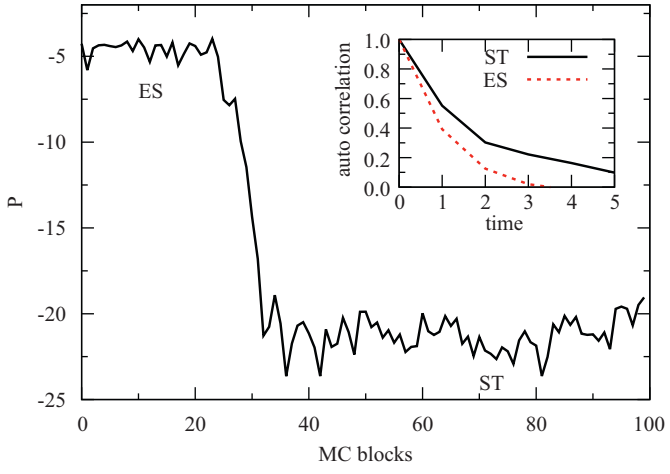


**Fig. 3.** At $S=60$ the results for the potential energy $\mathcal{P}$ at each MC block ($5\times10^3$ MCS) starting from an initial unlocalized path obtained by a previous simulation at $S=52.5$. We can see that after about 30 blocks there is a transition from the ES state to the ST state. In the inset is shown the autocorrelation function, defined in Eq. (A.8), for the potential energy, for the two states. The correlation time, in MC blocks, is shorter in the unlocalized phase than in the localized one. The computer time necessary to carry on a given number of Monte Carlo steps is longer for the unlocalized phase.

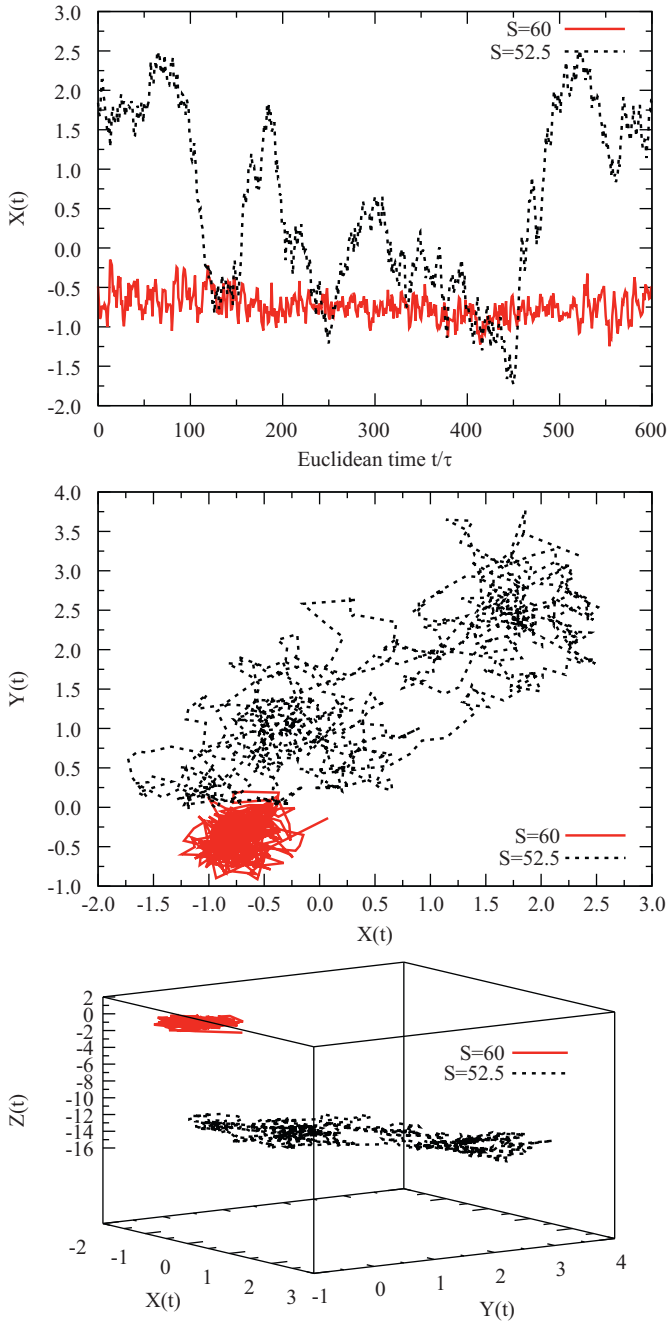


**Fig. 4.** The top panel shows the polaron (closed) path $x(t)$ as a function of Euclidean time $t$ in units of $\tau$ at equilibrium during the simulation. The middle panel shows the projection on the $x-y$ plane of the path. The bottom panel shows the three-dimensional path. We see clearly how both path has moved from the initial path located on the origin but the path at $S=52.5$ is much less localized than the one at $S=60$.

function (defined in Eq. (A.8)) which decay much more slowly in the ES state than in the ST state as shown in the inset of Fig. 3. Concerning the critical property of the transition between the ES and ST states our numerical results are in favor of the presence of a discontinuity in the potential energy. In the large β limit at $\beta=15$ and fixing the adiabatic coupling constant to $\gamma=0.02$, the ST state appears at a value of the coupling constant between $S=52.5$ and $S=55$. With the increase of β, the values for the potential energy $P=\langle\mathcal{P}\rangle$ increase in the weak coupling regime but decrease in the strong coupling region.

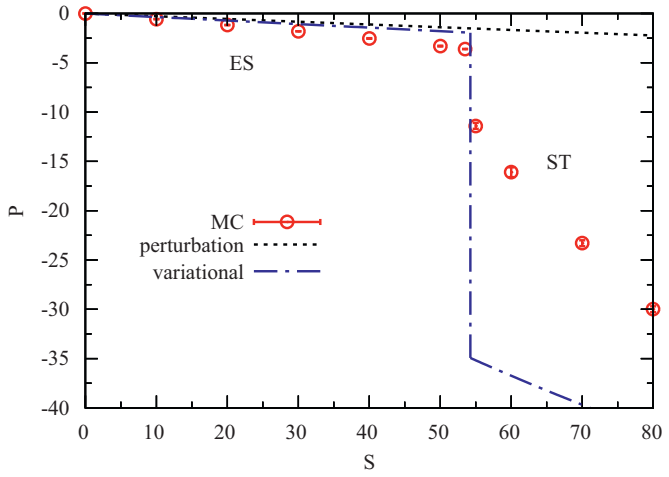


**Fig. 5.** Shows the behavior of the potential energy $P$ as a function of the coupling constant $S$. The points are the MC results (see Table 1), the dashed line is the second order perturbation theory result (perturbation) valid in the weak coupling regime and the dot-dashed line is the variational approach from Ref. [23] (variational) in the weak and strong coupling regimes.

From second order perturbation theory (see Ref. [12] Section 8.2) follows that the energy shift $E(\gamma,S)$ is given by $-3S\gamma[1/2-\gamma+\gamma^2\ln(1+1/\gamma)]$ from which one extracts the potential energy shift by taking $P(\gamma,S)=\gamma dE(\gamma,S)/d\gamma$. From the Feynman variational approach of Ref. [23] follows that in the weak regime the energy shift is $-3S\gamma[1/2-\gamma+\gamma\ln(1+1/\gamma)]$ and in the strong coupling regime $-S+3\sqrt{S/5}\gamma$.

## 9. Conclusions

We used for the first time a specialized path integral Monte Carlo method to study the low temperature behavior of an acoustic polaron. At an inverse temperature $\beta=15$ (close to the ground state of the polaron) and at a non-adiabatic parameter $\gamma=0.02$ typical of ionic crystals we found numerical evidence for a phase transition between an extended state in the weak coupling regime and a self-trapped one in the strong coupling regime at a value of the phonons–electron coupling constant $S=54.3(7)$. The transition also appears looking at the potential energy as a function of the coupling constant where a jump discontinuity is observed. Comparison with the perturbation theory and the variational calculation of Ref. [23] is also presented.

The specialized path integral Monte Carlo simulation method used as an unbiased way to study the properties of the acoustic polaron has been presented in full detail. It is based on the Lévy construction and the multilevel Metropolis method with correlated sampling. Some remarks on the estimation of the errors in the Monte Carlo calculation are also given in the Appendix. This complement our previous paper [26] where fewer details on the Monte Carlo method had been given.

Our method differs from previously adopted methods [29–34, 28,35]. Unlike the method of Ref. [29] our path integral is in real space rather than in Fourier space, Refs. [34,35] put the polaron on a lattice and not on the continuum as we did, while Refs. [33] use PIMC single slice move whereas the multilevel PIMC we used instead is a general sampling method which can efficiently make multislice moves. The efficiency $\xi$ (see the Appendix) for the potential energy increases respect to the single slice sampling because the coarsest movements are sampled and rejected before the finer movements are even constructed. In Ref. [28] the Lévy construction was used as in our case but the Metropolis test was performed after the entire path had been reconstructed, using an

effective action, and not at each intermediate level of the reconstruction. In Ref. [28] the simpler Levy reconstruction scheme was also found to be satisfactory for the efficient sampling of the polaron configuration space even at strong coupling. Even if we have not implemented the method of Ref. [28] we expect our method to be of comparable efficiency to the one of these authors. Infact it is true that the Levy construction is computationally cheap but guiding the path as it is been reconstructed starting already from the first levels as we did should have the advantage of refining the sampling since the path is guided through configuration space starting from the small displacements.

Although our results are of a numerical nature and we only probed the acoustic polaron for one value of the non-adiabatic parameter $\gamma$ we think that the analysis supports the existence of a localization phase transition as the phonons–electron coupling constant $S$ is increased at constant temperature or as the temperature is decreased at constant $S$. More so considering the fact that the introduction of a cut-off parameter has shown to work successfully in renormalization treatments.

## Appendix A. Estimating errors

Since asymptotic convergence is guaranteed, the main issue is whether configuration space is explored thoroughly in a reasonable amount of computer time. Let us define a measure of the convergence rate and of the efficiency of a given random walk. This is needed to compare the efficiency of different transition rules, to estimate how long the runs should be, and to calculate statistical errors.

The rate of convergence is a function of the property being calculated. Let $\mathcal{O}(s)$ be a given property, and let its value at step $k$ of the random walk be $\mathcal{O}_k$. Let the estimator for the mean and variance of a random walk with $N$ MCS be

$$O = \langle \mathcal{O}_k \rangle = \frac{1}{N}\sum_{k=0}^{N-1} \mathcal{O}_k, \tag{A.1}$$

$$\sigma^2(\mathcal{O}) = \langle (\mathcal{O}_k - O)^2 \rangle. \tag{A.2}$$

Then the estimator for the variance of the mean will be

$$\sigma^2(O) = \left\langle \left( \frac{1}{N}\sum_k \mathcal{O}_k - \frac{1}{N}\sum_k O \right)^2 \right\rangle, \tag{A.3}$$

$$\sigma^2(O) = \frac{1}{N^2}\left\langle \left[ \sum_k (\mathcal{O}_k - O) \right]^2 \right\rangle, \tag{A.4}$$

$$\sigma^2(O) = \frac{1}{N^2}\left\{ \sum_k \langle (\mathcal{O}_k - O)^2 \rangle + 2\sum_{i<j} \langle (\mathcal{O}_i - O)(\mathcal{O}_j - O) \rangle \right\}, \tag{A.5}$$

$$\sigma^2(O) = \frac{\sigma^2(\mathcal{O})}{N}\left\{ 1 + \frac{2}{N\sigma^2(\mathcal{O})}\sum_{i<j} \langle (\mathcal{O}_i - O)(\mathcal{O}_j - O) \rangle \right\}, \tag{A.6}$$

$$\sigma^2(O) = \frac{\sigma^2(\mathcal{O}) k_{\mathcal{O}}}{N}. \tag{A.7}$$

The quantity $k_{\mathcal{O}}$ is called the *correlation time* and can be calculated given the autocorrelation function for $A_k = \mathcal{O}_k - O$. The estimator for the *autocorrelation function*, $c_k$, can be constructed observing that in the infinite random walk, $\langle A_i A_j \rangle$ has to be a function of $|i-j|$ only. Thus the estimator can be written

$$c_k = \frac{\langle A_0 A_k \rangle}{\sigma^2(\mathcal{O})} = \frac{1}{(N-k)\sigma^2(\mathcal{O})}\sum_{n=1}^{N-k} A_n A_{n+k}. \tag{A.8}$$

So that the estimator for the correlation time will be

$$k_{\mathcal{O}} = 1 + \frac{2}{N}\sum_{k=1}^{N} (N-k) c_k. \tag{A.9}$$

To determine the true statistical error in a random walk, one needs to estimate this correlation time. To do this, it is very important that the total length of the random walk be much greater than $k_{\mathcal{O}}$. Otherwise the result and the error will be unreliable. Runs in which the number of steps $N \gg k_{\mathcal{O}}$ are called *well converged*.

The correlation time gives the average number of steps needed to decorrelate the property $\mathcal{O}$. It will depend crucially on the transition rule and has a minimum value of 1 for the optimal rule (while $\sigma(\mathcal{O})$ is independent of the sampling algorithm).

Normally the equilibration time will be at least as long as the equilibrium correlation time, but can be longer. Generally the equilibration time depends on the choice for the initial path. To lower this time is important to choose a physical initial path. Since the polaron system is isotropic, we chose the initial path with all time slices set to $\vec{0}$.

The efficiency of a random walk procedure (for the property $\mathcal{O}$) is defined as how quickly the error bars decrease as a function of the computer time, $\xi_{\mathcal{O}} = 1/\sigma^2(O)N\mathcal{T} = 1/\sigma^2(\mathcal{O})k_{\mathcal{O}}\mathcal{T}$ where $\mathcal{T}$ is the computer time per step. The efficiency depends not only on the algorithm but also on the computer and the implementation.

## References


[1] B. Gerlach, H. Löwen, Rev. Mod. Phys. 63 (1991) 63.
[2] J.T. Devreese, A.S. Alexandrov, Rep. Prog. Phys. 72 (2009) 066501.
[3] L.D. Landau, Phys. Z. Sowjetunion 3 (1933) 644.
[4] L.D. Landau, S. Pekar, Zh. eksper. teor. Fiz. 16 (1946) 341.
[5] L.D. Landau, S.I. Pekar, Zh. Eksp. Teor. Fiz. 18 (1948) 419.
[6] H. Fröhlich, H. Pelzer, S. Zienau, Phil. Mag. 41 (1950) 221.
[7] H. Fröhlich, Adv. Phys. 3 (1954) 325.
[8] R.P. Feynman, Phys. Rev. 97 (1955) 660.
[9] F.M. Peeters, J.T. Devreese, Phys. Stat. Sol. 112 (1982) 219.
[10] B.A. Mason, S. Das Sarma, Phys. Rev. B 33 (1986) 1412.
[11] T.K. Mitra, A. Chatterjee, S. Mukhopadhyay, Phys. Rep. 91 (1987) 153.
[12] R.P. Feynman, Statistical Mechanics, Benjamin, New York, 1972.
[13] Y. Osaka, Prog. Theor. Phys. 22 (1959) 437.
[14] Y. Osaka, J. Phys. Soc. Jpn. 21 (1965) 423.
[15] D.P.L. Castrigiano, N. Kokiantonis, Phys. Lett. 96A (1983) 55.
[16] D.P.L. Castrigiano, N. Kokiantonis, Phys. Lett. 104A (1984) 364.
[17] D.C. Khandekar, S.V. Lawande, Phys. Rep. 137 (1986) 115.
[18] Y-Sheng He, Pei-Heng Wu, Li-Fang Xu, Zong-Xian Zhao (Eds.), Proceedings of the International Conference on Materials & Mechanism of Superconductivity, High Temperature Superconductors V, Physica (Amsterdam) 282C–287C (1997).
[19] J. Tempere, W. Casteels, M.K. Oberthaler, S. Knoop, E. Timmermans, J.T. Devreese, Phys. Rev. B 80 (2009) 184504.
[20] Y. Toyozawa, Prog. Theor. Phys. 26 (1961) 29.
[21] C.G. Kuper, G.D. Whitfield (Eds.), Polarons and Excitons, Oliver and Boyd, Edinburgh, 1963, p. 211.
[22] F.M. Peeters, J.T. Devreese, Phys. Rev. B 32 (1985) 3515.
[23] A. Sumi, Y. Toyozawa, J. Phys. Soc. Jpn. 35 (1973) 137.
[24] D. Emin, T. Holstein, Phys. Rev. Lett. 36 (1976) 323.
[25] M.P.A. Fisher, W. Zwerger, Phys. Rev. B 34 (1986) 5912.
[26] R. Fantoni, Phys. Rev. B 86 (2012) 144304.
[27] D.M. Ceperley, Rev. Mod. Phys. 67 (1995) 279.
[28] J.T. Titantah, C. Pierleoni, S. Ciuchi, Phys. Rev. Lett. 20 (2001) 206406.
[29] C. Alexandrou, W. Fleischer, R. Rosenfelder, Phys. Rev. Lett. 65 (1990) 2615.
[30] C. Alexandrou, R. Rosenfelder, Phys. Rep. 215 (1992) 1.
[31] M. Crutz, B. Freedman, Ann. Phys. 132 (1981) 427.
[32] M. Takahashi, M. Imada, J. Phys. Soc. Jpn. 53 (1983) 963.
[33] X. Wang, Mod. Phys. Lett. B 12 (1998) 775.
[34] P.E. Kornilovitch, J. Phys.: Condens. Matter 9 (1997) 10675.
[35] P.E. Kornilovitch, J. Phys.: Condens. Matter 19 (2007) 255213.
[36] J. Bardeen, W. Shockley, Phys. Rev. 80 (1950) 72.
[37] R.P. Feynman, A.R. Hibbs, Quantum Mechanics and Path Integrals, McGraw-Hill, New York, 1965.
[38] P. Lévy, Compos. Math. 7 (1939) 283.
[39] D.M. Ceperley, E.L. Pollock, Phys. Rev. Lett. 56 (1986) 351.
[40] D.M. Ceperley, E.L. Pollock, Phys. Rev. B 39 (1989) 2084.
[41] J.M. Hammersley, C.D. Handscomb, Monte Carlo Methods, Chapman and Hall, London, 1964.